processes

MDPI

Article

Flowing Microreactors for Periodate/H_2O_2 Advanced Oxidative Process: Synergistic Degradation and Mineralization of Organic Dyes

Abderrahmane Talbi, Slimane Merouani * and Aissa Dehane

Laboratory of Environmental Process Engineering, Faculty of Process Engineering, University Constantine 3 Salah Boubnider, P.O. Box 72, Constantine 25000, Algeria; aissaleon15@gmail.com (A.D.)
* Correspondence: s.merouani@yahoo.fr

Abstract: The periodate/hydrogen peroxide (PI/H_2O_2) system is a recently developed advanced oxidation process (AOP) characterized by its rapid reaction kinetics, making it highly suitable for continuous-flow applications compared to conventional batch systems. Despite its potential, no prior studies have investigated its performance under flowing conditions. This work presents the first application of the PI/H_2O_2 process in a tubular microreactor, a promising technology for enhancing mass transfer and process efficiency. The degradation of textile dyes (specifically Basic Yellow 28 (BY28)) was systematically evaluated under various operating conditions, including reactant concentrations, flow rates, reactor length, and temperature. The results demonstrated that higher H_2O_2 flow rates, increased PI dosages, and moderate dye concentrations (25 µM) significantly improved degradation efficiency, achieving complete mineralization at 2 mM PI and H_2O_2 flow rates of 80–120 µL/s. Conversely, elevated temperatures negatively impacted the process performance. The influence of organic and inorganic constituents was also examined, revealing that surfactants (SDS, Triton X-100, Tween 20, and Tween 80) and organic compounds (sucrose and glucose) acted as strong hydroxyl radical scavengers, substantially inhibiting dye oxidation—particularly at higher concentrations, where nearly complete suppression was observed. Furthermore, the impact of water quality was assessed using different real matrices, including tap water, seawater, river water, and secondary effluents from a municipal wastewater treatment plant (SEWWTP). While tap water exhibited minimal inhibition, river water and SEWWTP significantly reduced process efficiency due to their high organic content competing with reactive oxygen species (ROS). Despite its high salt content, seawater remained a viable medium for dye degradation, suggesting that further optimization could enhance process performance in saline environments. Overall, this study highlights the feasibility of the PI/H_2O_2 process in continuous-flow microreactors and underscores the importance of considering competing organic and inorganic constituents in real wastewater applications. The findings provide valuable insights for optimizing AOPs in industrial and municipal wastewater treatment systems.

Keywords: Tubular microreactors; continuous-flow; textile dyes; advanced oxidation processes (AOPs); PI/H_2O_2 process; mineralization; organic additives; environmental matrices

check for updates

Academic Editors: Ruben Vasquez-Medrano, Dorian Prato-Garcia and Patricio J. Espinoza-Montero

Received: 14 March 2025
Revised: 20 April 2025
Accepted: 7 May 2025
Published: 13 May 2025

Citation: Talbi, A.; Merouani, S.; Dehane, A. Flowing Microreactors for Periodate/H_2O_2 Advanced Oxidative Process: Synergistic Degradation and Mineralization of Organic Dyes. *Processes* **2025**, *13*, 1487. https://doi.org/10.3390/pr13051487

Copyright: © 2025 by the authors. Licensee MDPI, Basel, Switzerland. This article is an open access article distributed under the terms and conditions of the Creative Commons Attribution (CC BY) license (https://creativecommons.org/licenses/by/4.0/).

1. Introduction

Periodate (PI; IO_4^-) has been utilized for the oxidative cleavage of specific chemical bonds, such as the 1,2-glycol linkage in carbohydrates [1], as well as for the selective oxidation of amines [2] and sulfides [3] into aldehydes and sulfoxides, respectively. PI,

with a moderate oxidizing potential, $E^0(IO_4^-/IO_3^-)$ = 1.7 V vs. NHE [4], has demonstrated its ability to oxidize substituted phenols [5] and serve as a disinfectant against bacteria. However, the PI-driven oxidative process is largely selective, as many chemicals exhibit complete resistance to oxidation [6–11], and its application is primarily limited to pollutant transformation rather than mineralization.

Recent advancements in environmental water remediation have revealed that PI can be converted into highly reactive intermediates, shedding light on a specialized treatment approach known as periodate-based advanced oxidation processes (PI-based AOPs) [12–14]. PI-based AOPs have garnered significant interest in recent years, largely due to their effectiveness in degrading and mineralizing a wide range of organic pollutants while producing iodate (IO_3^-) as an environmentally benign byproduct [7,15–18]. Periodate can be activated through various pathways, including energy sources (e.g., UV light and ultrasound) [11,19] reduced transition-metal ions (e.g., Mn^{2+} and Fe^{2+}) [20,21] metal oxides [16,22] and non-metallic reductants (e.g., hydroxylamine and H_2O_2) [15,23]. These activation methods confirmed the formation of reactive species (RS), such as iodate radicals ($IO_3^{\bullet}$), hydroxyl radicals ($^{\bullet}OH$), superoxide radicals ($O_2^{\bullet-}$), singlet oxygen ($^1O_2$), and high-valent iron-oxo species (e.g., Fe(IV)) [6,11,15,16,19–22]. While these RS are generally believed to enhance the oxidative potential of periodate, the overall effectiveness of PI-based AOPs is strongly influenced by operational conditions (especially pH reagents loading) and water matrix components.

The PI/H_2O_2 system was firstly identified by Chadi et al. [23,24] in 2019 as a promising and highly effective periodate-based AOP for the degradation and mineralization of micropollutants in aqueous solutions. Their findings demonstrated that the interaction between H_2O_2 and periodate occurs instantaneously, generating a suite of potent reactive species, including $^{\bullet}OH$, $O_2^{\bullet-}$, $^1O_2$, $IO_3^{\bullet}$, and $IO_4^{\bullet}$ [23]. This process exhibited remarkable efficiency in removing toluidine blue (TB) dye within an extremely short reaction time. The key reactions governing the PI/H_2O_2 system are summarized in Table 1 [23]. To elucidate the role of reactive species, radical scavengers such as ascorbic acid, tert-butanol, 2-propanol, sodium azide, and phenol were employed [23]. Scavenging tests confirmed the formation of $^{\bullet}OH$, $^1O_2$, and $O_2^{\bullet-}$,with hydroxyl radicals playing a dominant role in TB degradation at pH 5.4. Notably, TB removal at pH 5.4 dropped from 73% to approximately 9% (i.e., an 87% decrease) upon the addition of 100 mM tert-butanol, a selective $^{\bullet}OH$ scavenger. Meanwhile, $O_2^{\bullet-}$ appeared to act primarily as a precursor to other free radicals [23]. The influence of operational parameters—including pH, temperature, and initial concentrations of periodate, H_2O_2, and TB—as well as the effects of organic and inorganic additives and water matrix composition, was thoroughly examined in the original studies [23,24]. Overall, the system exhibits behavior similar to other hydroxyl radical-based AOPs in terms of reactivity. However, a distinctive feature of this process is the rapid initial pollutant degradation, leading to an immediate and stable final concentration. Subsequent studies involving various micropollutants—including benzoic acid, bisphenol A, 4-chlorophenol, phenol, nitrobenzene, 4-nitrobenzoic acid, and naproxen—have confirmed the exceptional speed of this process [17,18] and its superiority over other PI-based AOPs, particularly PI/UV and PI/nFe^0-Ni [17].

Table 1. Reaction mechanism for PI/H_2O_2 system at pH~5 [23,24].

Reaction	**n°**
$IO_4^- + H_2O_2 \rightarrow IO_3^{\bullet} + O_2^{\bullet-} + H_2O$	(1)
$H_2O_2 + O_2^{\bullet-} \rightarrow {}^{\bullet}OH + OH^- + {}^1O_2$	(2)
$IO_4^- + 2O_2^{\bullet-} + H_2O \rightarrow 2{}^1O_2 + IO_3^- + 2\ OH^-$	(3)
$2O_2^{\bullet-} + 2H_2O \rightarrow {}^1O_2 + H_2O_2 + 2OH^-$	(4)

Table 1. *Cont.*

Reaction	n°
$O_2^{\bullet-} + {}^{\bullet}OH \rightarrow {}^1O_2 + OH^-$	(5)
${}^{\bullet}OH + {}^{\bullet}OH \rightarrow H_2O_2$	(6)
${}^1O_2 \rightarrow {}^3O_2 + h\nu$ (λ = 643 nm)	(7)
${}^1O_2 + {}^1O_2 \rightarrow ({}^1O_2)_2{}^* \rightarrow 2({}^3O_2) + h\nu$ (λ = 478 nm)	(8)
$O_2^{\bullet-} + H^+ \rightleftharpoons HO_2^{\bullet}$ $pK_a = 4.8$	(9)
$H_2O_2 + {}^{\bullet}OH \rightarrow HO_2^{\bullet} + H_2O$	(10)
$IO_4^- + IO_3^{\bullet} \rightarrow IO_4^{\cdot} + IO_3^-$	(11)
$IO_3^{\bullet} + IO_3^{\bullet} \rightarrow I_2O_6$	(12)
$I_2O_6 + H_2O \rightarrow IO_4^- + IO_3^- + 2H^+$	(13)
$IO_4^{\cdot} + IO_4^{\cdot} \rightarrow I_2O_8$	(14)
$I_2O_8 + H_2O \rightarrow IO_4^- + IO_3^- + 2H^+ + O_2$	(15)
$IO_4^- + {}^{\bullet}OH \rightarrow IO_4^{\bullet} + OH^-$	(16)

Recent studies have sparked debate regarding the reactive species involved in the PI/H_2O_2 system. Kim et al. [17] reexamined the mechanisms governing organic contaminant degradation in the PI/H_2O_2 process using EPR spin-trapping techniques. Their findings suggested that $^{\bullet}OH$ was the predominant ROS at pH < 5.0, while $^1O_2$ became dominant at higher pH values. The authors attributed the pH-dependent decontamination efficiency of the PI/H_2O_2 process to this shift in dominant ROS from $^{\bullet}OH$ to $^1O_2$ at pH 6.0. However, given that benzoic acid is not readily oxidized by $^1O_2$ [25], its removal at pH 6.0 indicates that $^{\bullet}OH$ likely remains a key contributor to degradation at this pH [17]. Furthermore, Kim et al. [17] proposed that superoxide radicals ($O_2^{\bullet-}$) act as crucial intermediates in the PI/H_2O_2 system, reacting with periodate to generate hydroxyl radicals via the following reaction:

$$IO_4^- + O_2^{\bullet-} + H_2O \rightarrow {}^{\bullet}OH + IO_3^- + O_2 + OH^- \quad (17)$$

According to Kim et al. [17], reaction (17) serves as the primary pathway for $^{\bullet}OH$ generation under acidic conditions (pH < 5), contradicting the mechanism proposed by Chadi et al. (Equations (1) and (2) in Table 1) [23,24]. However, other researchers have reported that $O_2^{\bullet-}$ predominantly facilitates the formation of $^1O_2$ [26], further complicating the mechanistic understanding of ROS evolution in the PI/H_2O_2 system. To clarify these discrepancies, Chen et al. [18] reinvestigated the influence of pH on the decontamination performance of the PI/H_2O_2 process, emphasizing the role of $H_4IO_6^-$. Their results demonstrated that increasing the pH from 2.0 to 10.0 significantly accelerated the degradation rate of organic contaminants but reduced overall removal efficiency. This pH-dependent trend closely correlated with the $^{\bullet}OH$ yield and the speciation of periodate. Specifically, while $^1O_2$ was detected at pH 9.0, $^{\bullet}OH$ remained the predominant oxidizing species across all tested pH conditions (pH 2–10), challenging the conclusions drawn by Kim et al. [17].

Anyway, a common agreement among key investigations (Chadi et al. [23,24], Kim et al. [17], and Chen et al. [18]) is the predominance of the $^{\bullet}OH$-driven pathway for pH values up to 5, as well as the rapid degradation capability of the PI/H_2O_2 process. The reaction occurs within a short time, making batch operation an unsuitable mode for optimal performance. Instead, continuous operation may yield superior results. However, careful consideration must be given to optimizing agitation system to enhance mass transfer efficiency and ensure effective pollutant degradation.

In this context, microreactors present a promising alternative for implementing the PI/H_2O_2 process. These advanced reactors offer enhanced mass and heat transfer, precise control over reaction conditions, and improved energy efficiency [27]. Microreactors, also known as microfluidic devices, are engineered to regulate chemical reactions and fluid dy-

namics through microchannels typically ranging in size from 1 µm to 1 mm [28]. Compared to conventional reactors, microreactors provide several advantages, including compact design, high surface-to-volume ratios, and reduced diffusion and conduction distances, leading to improved heat and mass transfer efficiency and laminar flow conditions [27]. These features facilitate efficient radical generation and pollutant degradation in a well-controlled environment, addressing some of the limitations of traditional reactor systems. However, despite their potential, microreactors remain underexplored in the field of AOPs, with limited studies assessing their feasibility for water treatment applications [29].

The present work reports the first application of the PI/H_2O_2 process in a flowing microreactor, demonstrating its efficiency in micropollutant degradation and mineralization. A tubular microreactor (2–6 m in length, 1 mm in diameter) submerged in a temperature-controlled water bath was utilized to facilitate the reaction between PI and H_2O_2 for persistent-textile dyes degradation. Special focus was given to Basic Yellow 28, an azo dye highly resistant to direct oxidation by either PI or H_2O_2 alone and non-biodegradable, making its removal from the environment particularly challenging. The removal of synthetic dyes, especially azo compounds, has received considerable attention due to their widespread use, complex structures, and potential toxicity [30,31]. The present work investigates the influence of key parameters, including flow conditions (PI, dye, and H_2O_2 concentrations), pH, temperature, reactor length, dissolved salts, organic matter, and various water matrices (tap water, treated wastewater, seawater, and river water) on dye conversion. Mineralization tests were conducted under specific conditions to confirm complete degradation of the dye. The obtained results were analyzed in depth, with a particular focus on the effectiveness of this newly adopted approach.

2. Material and Methods

2.1. Reagents

The dyes used as pollutants, along with their characteristics and suppliers, are presented in Table 2. All dyes were used as received without further purification. Hydrogen peroxide (35% *v*/*v*), sodium periodate, surfactants (Tween 20, Tween 80, Triton X-100, and sodium dodecyl sulfate [SDS]), glucose, sucrose, sodium hydroxide, and sulfuric acid (all supplied by Sigma-Aldrich, Saint Louis, MO, USA) were used as received.

Table 2. Main characteristics of dyes used in this study.

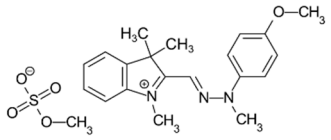
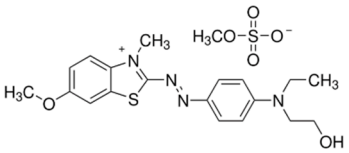
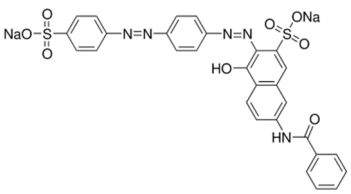
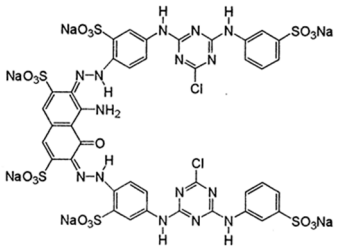
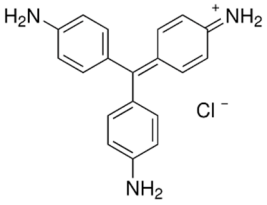
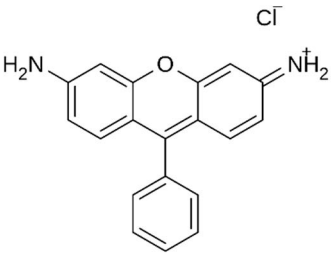
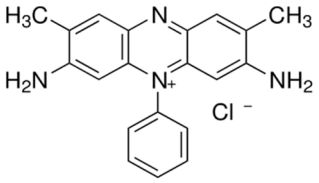
Dye (Abbreviation)	Calss	CAS Number	Formula (MW)	Molecular Structure	λ_{max} (Vis.)	Supplier
Basic Yellow 28 (BY28)	mono-azo dye	54060-92-354060-92-3	$C_{21}H_{27}N_3O_5S$ (433.5 g/mol)		438 nm	SAFILCO * (local textile manufacture)
Basic Blue 41 (BB41)	mono-azo dye	12270-13-2	$C_{19}H_{23}N_4O_2S.CH_3O_4S$ (482.57 g/mol)		612 nm	SAFILCO (local textile manufacture)
Direct Red 81 (DR81)	di-azo dye	2610-11-9	$C_{29}H_{19}N_5Na_2O_8S_2$ (675.6 g/mol)		507 nm	Sigma-Aldrich

Table 2. *Cont.*

Dye (Abbreviation)	Calss	CAS Number	Formula (MW)	Molecular Structure	λ_{max} (Vis.)	Supplier
Reactive Green 19 (RG19)	di-azo dye	68110-31-6	$C_{40}H_{23}Cl_2N_{15}Na_6O_{19}S_6$ (1418.94 g/mol)		628 nm	Sigma-Aldrich
Basic Fuchsin (BF)	triarylmethane dye	569-61-9	$C_{19}H_{17}N_3 \cdot HCl$ (323.82 g/mol)		547 nm	Sigma-Aldrich
Rhodamine B (RhB)	Xanthene dye	81-88-9	$C_{28}H_{31}ClN_2O_3$ (479.02 g/mol)		553 nm	Sigma-Aldrich
Safranine O (SO)	phenazine-based dye	477-73-6	$C_{20}H_{19}ClN_4$ (350.84 g/mol)		518 nm	Sigma-Aldrich

* Aurassienne Spinning and Blankets Company (SAFILCO), Ain Djasser, Algeria.

Seawater samples were collected from the Mediterranean Sea along the north-eastern coast of Algeria (Skikda) using pre-cleaned polyethylene bottles, approximately 1 m from the shoreline and at a depth of 20–30 cm to avoid surface contaminants. Wastewater samples were taken during dry weather conditions from the final effluent (prior to chlorination) of a secondary-treated municipal wastewater treatment plant (SEWWTP) located in the Constantine region (Algeria). All samples were transported immediately to the laboratory in cooled containers (4 °C), filtered through a 1 µm GA-100 glass fiber filter to remove suspended solids, and stored in clean bottles under refrigeration until use (typically within 48 h). Table 3 presents the key physicochemical characteristics of these water matrices.

Table 3. Main characteristics (before pH adjustment) of river water, tap water, seawater, and SWEWTP used in this study.

	River Water	Tap Water	Seawater	SEWWTP [a]
pH	7.4	7.3	7.6	7.6
Ca^{2+}	59.0 mg L^{-1}	78 mg L^{-1}	0.4 g L^{-1}	
Mg^{2+}	45.0 mg L^{-1}	-	1.3 g L^{-1}	
Na^{+}	15.0 mg L^{-1}	29 mg L^{-1}	11.0 g L^{-1}	Salinity = 0.8/L
K^{+}	2.0 mg L^{-1}	2.0 mg L^{-1}	-	
Cl^{-}	22.0 mg L^{-1}	40.0 mg L^{-1}	20.0 g L^{-1}	

Table 3. *Cont.*

	River Water	Tap Water	Seawater	SEWWTP [a]
SO_4^{2-}	40.0 mg L^{-1}	95.0 mg L^{-1}	3.0 g L^{-1}	
HCO_3^-	378.2 mg L^{-1}	~400 mg L^{-1}	-	
Br^-	0	0	65–80 mg/L	
COT [b]	0	0	~1.2–1.5	
COD [c]	0	0	2.71–4.69 mg/L	
BOD_5 [d]	0	0	1.78–2.92 mg/L	15 mg/L

[a] SEWWTP: Secondary effluent of wastewater treatment plant. [b] TOC: total organic carbon. [c] COD: chemical oxygen demand. [d] BOD_5: biological oxygen demand.

2.2. Experimental Setup

The experimental setup is schematically illustrated in Figure 1. The experiments were conducted using a tubular microreactor with an internal diameter of 1 mm and a total length of either 2 m or 6 m, coiled into a spiral configuration and fully submerged in a thermostatic water bath (50 × 50 × 30 cm^3) with precise temperature control (using JP Selecta Thermostat). The reactor was made from aluminum tubing with a wall thickness of 1 mm, ensuring efficient heat transfer.

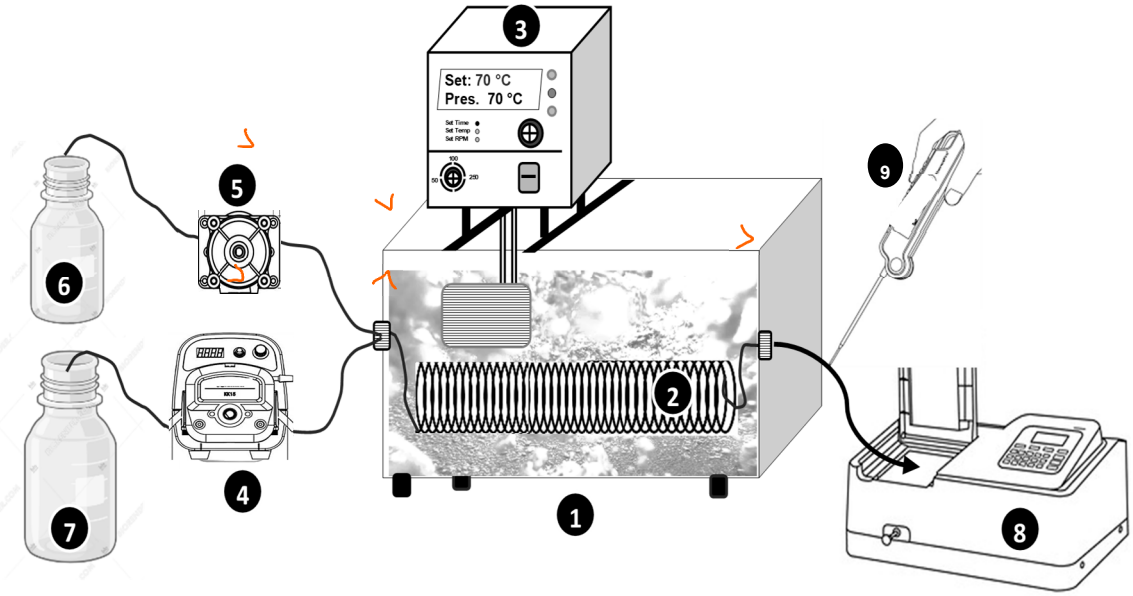


Figure 1. Schematic representation of the experimental setup for the process. (**1**) Water bath. (**2**) Microtubular reactor. (**3**) Heating thermostat (temperature control). (**4**) Peristaltic pump. (**5**) Micro-pump. (**6**) Oxidant's bottle. (**7**) Dye solution bottle. (**8**) Spectrophotometer (UV-Vis. Jenway 7205). (**9**) Themometer.

The reactor was fed with two separate solution streams:

1. Dye Solution Stream: This stream consists of a dye solution containing periodate, which was supplied to the reactor using a peristaltic pump (Master Flex Console Drive 7520-47) at a controlled flow rate of Q_{dye} = 278, 565, or 1100 µL/s. The dye concentration and periodate concentration in this stream were fixed at C_0 = 25 µM and $[PI]_{in}$ = 1 mM, although some runs were conducted at C_0 = 12.5 and 50 µM and $[PI]_{in}$ = 0.5–2 mM (tests of PI and C_0 impacts). Notably, the reactivity between the dye and periodate is negligible, which is why periodate was introduced within the dye stream.

2. Oxidant Solution Stream: A hydrogen peroxide (H_2O_2) solution with an initial concentration of 50 mM was supplied to the reactor at a controlled flow rate (Q_{H2O2} = 40, 80, and 120 µL/s) using a peristaltic micropump (Ismatec ISM640-0254).

Both steams were mixed at the reactor inlet using a T-mixer before entering the reactor. The reaction temperature was controlled by adjusting the water bath to the desired value, enabling a systematic investigation of thermal effects on reaction kinetics. The feed solutions (streams) temperature was 17–18 °C before entering the reactor.

2.3. Procedures

Solutions of dye, PI, and H_2O_2 were prepared using deionized water, except for tests involving different matrices, where only the dye solution was prepared in the respective matrix. To assess the impact of pH, all solutions, including the oxidant (H_2O_2) and dye (with PI), were pre-adjusted to the desired pH before running each experiment. The pH was adjusted using NaOH (0.1 or 1 M) or H_2SO_4 (0.1 or 1 M) as needed. To assess the impact of different water matrices on dye degradation, dye solutions were prepared in these matrices under the same conditions as those used for deionized water experiments. Matrices such as river water and wastewater (Table 3) were readably filtered multiple times before use in runs.

The dyes concentrations at the reactor inlet and outlet were measured at their maximum absorption wavelengths (mentioned in Table 2) using a Jasco V-730 UV-visible spectrophotometer. Calibration curves were established for each dye, based on the Beer-Lambert law ($Abs = \varepsilon LC$), ensuring accurate concentration determination. Each experimental run was conducted in triplicate, and the mean values were incorporated into the figures presenting 95% confidence of the results. The dye conversion at the reactor outlet was measured after a steady-state regime was attained (constant outlet concentration) using

$$X_{dye} = \frac{F_{dye,in} - F_{dye,out}}{F_{dye,in}} = \frac{Q_{dye,in}C_{dye,in} - Q_{out}C_{dye,out}}{Q_{dye,in}C_{dye,in}} \quad (18)$$

where $F_{dye,in}$ ($F_{dye,out}$) and $C_{dye,in}$ ($C_{dye,out}$) represent the molar flux and concentration of the dye at the reactor inlet (outlet), respectively. Additionally, Q_{in} denotes the volumetric flow rate of the inlet dye solution, and Q_{out} is the volumetric flow rate of the treated effluent at the reactor outlet.

3. Results and Discussion

3.1. PI and H_2O_2 Reactivity with BY28: Microreactor Flowing Conditions

Experiment runs were first conducted using PI and H_2O_2 separately to assess their effectiveness in degrading Basic Yellow 28 (BY28) within a flowing conditions under varying oxidant flow rates (40, 80, and 120 µL/s) and inlet pH conditions (3–11), while maintaining a constant dye flow rate of 565 µL/s. Across all tested conditions, dye conversion remained very low (Figure 2), confirming the dye's strong resistance to direct oxidation with molecular PI and H_2O_2. For PI, the highest degradation efficiency (13.96%) was observed at pH 7 and 40 µL/s, with comparable values at pH 9 (12%) and pH 11 (13%). Increasing the flow rate to 80 and 120 µL/s resulted in minor variations, with maximum conversion reaching 13.37% at pH 9 for 80 µL/s and 12.63% at pH 11 for 120 µL/s. Similarly, H_2O_2 exhibited its highest conversion of 15% at pH 9 and 40 µL/s, though efficiency declined significantly at pH 11 (7.49%). At 80 µL/s, degradation peaked at 13.52% for pH 9 but dropped to 3.31% at pH 11. The highest flow rate of 120 µL/s led to degradation efficiencies ranging between 8.91% and 13.67%, following a similar trend to PI. Overall, these findings highlight the persistent nature of BY28 and confirm that its oxidation by PI or H_2O_2 alone is unlikely, eliminating direct oxidation as the primary mechanism in the efficient hybrid

PI/H_2O_2 system. Similar low removals were obtained by PI and H_2O_2, separately, for all dye mentioned in Table 1. These conclusions align with batch-mode results obtained for Toluidine Blue [23] and several other micropollutants [17,18,32].

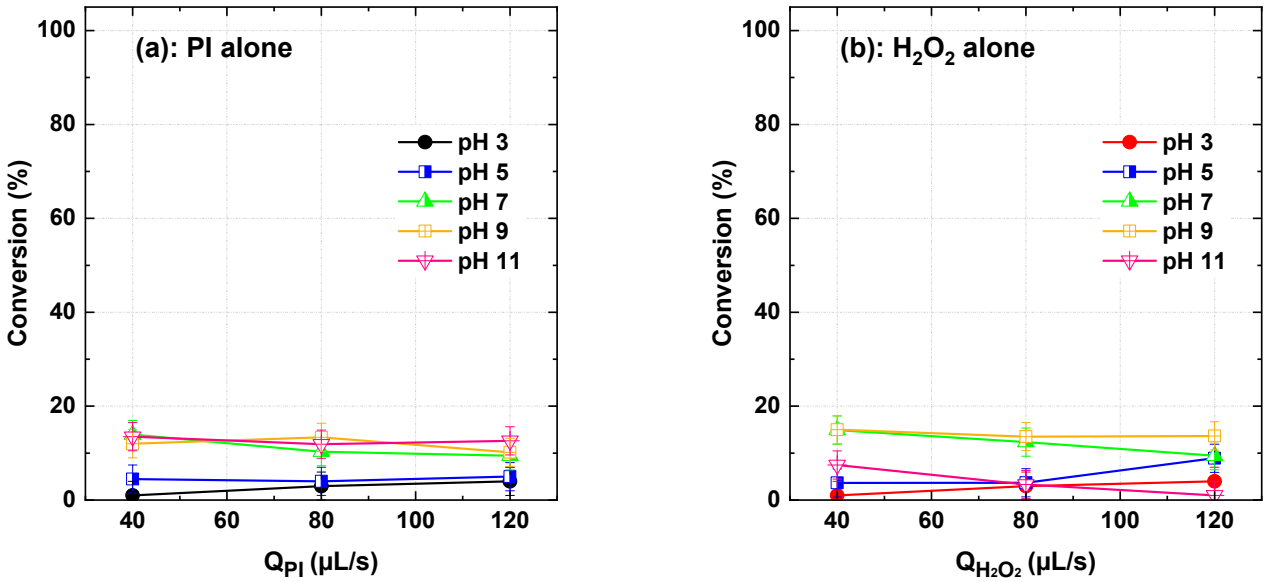


Figure 2. BY28 conversion using PI and H_2O_2 separately at varying flow rates and inlet pH conditions (dye solution and oxidants), with a constant dye flow rate of 565 µL/s. In these experiments, either PI or H_2O_2 was introduced (flowed) from the oxidant reservoir, while the dye was supplied through a separate stream (fresh dye solution). Reactor length L = 2 m.

Although recent studies [33,34] have demonstrated the potential of aluminum surfaces to catalyze the decomposition of H_2O_2 into hydroxyl radicals under highly acidic conditions and prolonged reaction times, such a side reaction is unlikely under our experimental conditions. The microreactor, although uncoated, operates with very short residence times (usually <10 s) and at moderately acidic pH levels (typically around pH 5), which are not conducive to aluminum–H_2O_2 interactions that generally require strong acidity and extended reaction durations (hours). This conclusion is further supported by control experiments (see Figure 2) and supplementary batch tests conducted in aluminum containers (100 mL, 20 ppm dye, pH 3, 500 µM H_2O_2, reaction time: 1 h), which showed negligible dye removal. Collectively, these observations confirm that the PI/H_2O_2 reactivity reported in this work is not influenced by any aluminum-induced side reactions.

3.2. PI/H_2O_2 Efficiency: Critical Role of pH

The efficiency of the PI/H_2O_2 system was investigated under varying inlet solution pH (3–11) and H_2O_2 flow rates (40, 80, and 120 µL/s). The PI concentration (1 mM) was kept constant, and it was co-fed with the dye solution at 565 µL/s, while the bath temperature was maintained at 25 °C. The results, presented in Figure 3, highlight the crucial impact of pH and H_2O_2 flow rate on the efficiency of this hybrid process.

The highest dye conversion was achieved at acidic to near acidic conditions (pH 3 and 5), with maximum degradation observed at 120 µL/s H_2O_2 flow rate (96.7% and 91.3%, respectively). Notably, at pH 3, conversion improved steadily with increasing H_2O_2 flow rate: from 38.1% (40 µL/s) to 84.2% (80 µL/s) and 96.7% (120 µL/s), suggesting that acidic conditions favor periodate activation. At neutral conditions (pH 7), the process remained moderately effective, with dye conversion ranging between 31.0% (40 µL/s) and 39.6% (120 µL/s). However, the efficiency dropped significantly at alkaline pH (9 and 11), where conversion barely exceeded 20%, regardless of the H_2O_2 flow rate. Interestingly,

the observed values at pH 9 and 11 (~15–24%) align closely with the arithmetic sum of the individual PI and H_2O_2 impacts, indicating a loss of process performance at higher pH. This pH-dependent trend is consistent with previous batch-mode studies. Chadi et al. [23] reported similar behavior for Toluidine Blue degradation (H_2O_2: 10–50 mM), while Kim et al. [17] observed comparable effects for 4-chlorophenol and benzoic acid removal (H_2O_2: 0.5–10 mM). However, Chadi et al. [17] noted a decline in efficiency above 50 mM H_2O_2, identifying an optimal peroxide dosage for batch experiments. In contrast, no such inhibition was observed in our continuous-flow system, likely due to the controlled dilution of H_2O_2 from the stock solution (50 mM), preventing excessive scavenging effects.

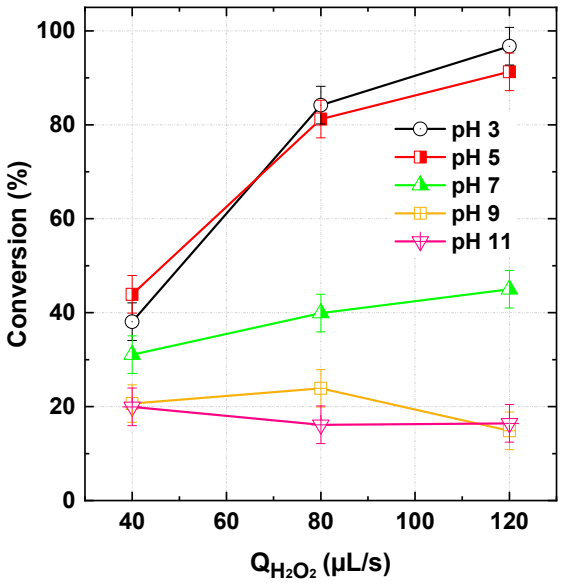


Figure 3. BY28 conversion with the PI/H_2O_2 system in the flowing microreactor as a function of H_2O_2 flow rate and pH of the inlet solution streams (Q_{feed} = 565 µL/s with $C_{dye,in}$ = 25 µM and $[PI]_{in}$ = 1 mM, Reactor length L = 2 m).

To better understand the impact of pH, it is essential to consider the reactive species involved in the PI/H_2O_2 system and how pH influences their distribution. As discussed in the introduction, previous studies have debated the dominant reactive species in this process. Chadi et al. [23], the pioneers of this process, reported that •OH radicals play a major role, with only a minor contribution from singlet oxygen ($^1O_2$) and IO_3• radicals. In contrast, Kim et al. [17] found that IO_3• has no significant role in the process, while $^1O_2$ dominates at pH > 6, with •OH radicals being the primary species at lower pH. Similarly, Chen et al. [18] reported that •OH radicals remain dominant across a wide pH range (2–10), despite the presence of $^1O_2$ in alkaline solutions. While a unanimous consensus on the contribution of each reactive species has not yet been established, there is strong agreement on the crucial role of •OH radicals in the process in the multiple studies. Moreover, Shah et al. [35] also confirmed the roles of •OH and $^1O_2$ in the KIO_4/H_2O_2 chemiluminescent system using EPR spin trapping and chemical probe analysis. In the following section, we will interpret our pH-dependent results by considering only •OH and $^1O_2$, since the involvement of IO_3• has been ruled out based on the findings of Kim et al. [17] and Chen et al. [23].

The solution pH significantly influences the species-distribution diagram of both IO_4^- and H_2O_2, which in turn modulates the distribution of reactive species. IO_4^- is the dominant species at pH < 8, while at higher pH, it predominantly dimerizes into $H_2I_2O_{10}^{4-}$ [36–38]. Bokar and Choi [26] found that IO_4^- is more effective than its dimerized form in generating $^1O_2$. Consequently, the concentration of $^1O_2$ (on considered ROS) is

expected to be lower at alkaline pH. In parallel, as the pH increases, HO_2^- ions emerge due to the deprotonation of H_2O_2 (pK_a = 11.75). This results in an additional reaction between HO_2^- and H_2O_2 (Equation (19)), which may deplete available peroxide in the system [39]. Notably, $^{\bullet}OH$ reacts rapidly with HO_2^- (Equation (20), $k = 7.5 \times 10^9$ $M^{-1}s^{-1}$) [40], nearly 100 times faster than their reaction with H_2O_2 (Equation (10), $k = 2.7 \times 10^7$ $M^{-1}s^{-1}$) [40], further reducing the effectiveness of $^{\bullet}OH$-mediated oxidation.

$$H_2O_2 + HO_2^- \rightarrow H_2O + O_2 + OH^- \quad (19)$$

$$HO_2^- + {}^{\bullet}OH \rightarrow OH^- + HO_2^{\bullet} \quad (20)$$

At high pH, $^{\bullet}OH$ radicals are further deactivated by hydroxide ions (Equation (21)), where the reaction rate ($k = 1.2 \times 10^{10}$ $M^{-1}s^{-1}$) is significantly higher than its reverse reaction ($k = 10^8$ s^{-1}). Furthermore, hydrogen peroxide undergoes enhanced self-decomposition (Equation (22)) in alkaline media, leading to a decline in available H_2O_2 [39].

$$^{\bullet}OH + OH^- \rightleftharpoons O^{\bullet-} + H_2O \quad pK_a = 11.9 \quad (21)$$

$$2H_2O_2 \rightarrow 2H_2O + 2O_2 \quad (22)$$

According to Chadi et al. [23], ROS Scavenging of by bicarbonate (HCO_3^-) and carbonate (CO_3^{2-}) ions represents another possible pathway that limits dye degradation at pH 9 and 11 (Figure 3). Under alkaline conditions, dissolved CO_2 primarily exists as HCO_3^- (pH > pK_{a1} = 6.35) or CO_3^{2-} (pH > pK_{a1} = 10.33), both of which readily react with $^{\bullet}OH$ (Equations (23) and (24)) and $O_2^{\bullet-}$ (Equations (25) and (26)), leading to the formation of $CO_3^{\bullet-}$ radicals [10,41,42]. Since $CO_3^{\bullet-}$ is considerably less reactive than $^{\bullet}OH$, its formation results in diminished oxidative capacity. Furthermore, the reaction rate of CO_3^{2-} with $^{\bullet}OH$ (3.9×10^8 $M^{-1}s^{-1}$) is approximately 46 times higher than that of HCO_3^- with $^{\bullet}OH$, indicating that radical quenching becomes increasingly significant at pH > 10.

$$HCO_3^- + {}^{\bullet}OH \rightarrow CO_3^{\bullet-} + H_2O \quad (23)$$

$$CO_3^{2-} + {}^{\bullet}OH \rightarrow CO_3^{\bullet-} + OH^- \quad (24)$$

$$HCO_3^- + O_2^{\bullet-} \rightarrow CO_3^{\bullet-} + HO_2^- \quad (25)$$

$$CO_3^{2-} + O_2^{\bullet-} \rightarrow CO_3^{\bullet-} + O_2^{2-} \quad (26)$$

Based on the above mechanisms, increasing the pH reduces the overall concentration of key reactive species due to several processes (e.g., speciation effects, ROS deactivation, H_2O_2 decomposition, and radical scavenging by carbonate species). Consequently, the optimal pH range for efficient dye degradation in the PI/H_2O_2 system under flow conditions appears to be acidic to near-neutral (pH 3–5), similar to findings in batch-mode operations.

According to the results in Figure 3, dye conversion at pH 3–5 increases with the H_2O_2 flow rate. This trend is logical, as a higher flow rate supplies more H_2O_2, enhancing the generation of ROS, particularly $^{\bullet}OH$, which are primarily responsible for dye degradation at acidic conditions [17,23]. The increased availability of H_2O_2 also sustains the chain reactions involved in radical production, leading to a higher oxidative capacity in the system. Acidic conditions suppress the formation of less reactive oxygen species, such as superoxide anions ($O_2^{\bullet-}$). Moreover, the decomposition of H_2O_2 is slower at low pH, ensuring a sustained ROS generation over time. This explains why the increase in dye degradation efficiency is more pronounced within this pH range. In contrast, the enhanced decomposition of H_2O_2 in alkaline conditions limits its availability for ROS production, further reducing the system's overall oxidative performance.

3.3. Radicals Probing

Figure 4 presents the results of radical probing tests conducted using excess of tert-butanol (*t*-BuOH: 100 mM) and benzoic acid (BA: 1 mM), which were initially mixed into the dye stock solution during the flowing runs (565 µL/s dye, 120 µL/s H_2O_2) at pH 5. *t*-BuOH is a well-known scavenger of •OH radicals, with a high biomolecular second-order rate constant of 6×10^8 $M^{-1}s^{-1}$ [40], but it remains completely unreactive toward IO_3• [7,22,43]. As observed, the presence of *t*-BuOH completely suppressed the beneficial effect of the PI/H_2O_2 process across the tested H_2O_2 flow rates (Figure 3). This confirms the crucial role of hydroxyl radicals in the oxidative degradation of the dye while ruling out any significant contribution from IO_3•. These findings are further supported by Kim et al. [17], who investigated the degradation of benzoic acid (BA) in the PI/H_2O_2 process using t-BuOH and methanol as specific •OH scavengers. Their study demonstrated that both alcohols completely suppressed BA oxidation, highlighting the crucial role of •OH radicals.

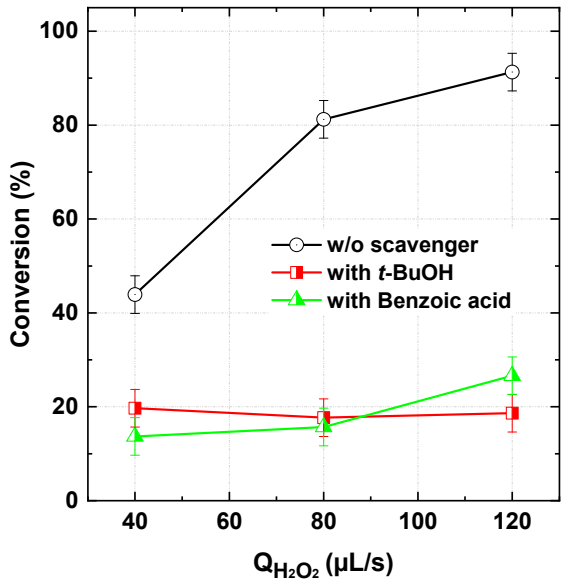


Figure 4. Radicals probing tests with tert-butanol (t-BuOH: 100 mM) and Benzoic acid (BA: 1 mM) during BY28 degradation with the PI/H_2O_2 system in the flowing microreactor (Q_{feed} = 565 µL/s with $C_{dye,in}$ = 25 µM $[PI]_{in}$ = 1 mM, and $[scavenger]_{in}$ = 100 mM for *t*-BuOH and 1 mM for BA, pH_{in} 5, Reactor length L = 2 m).

Similarly, benzoic acid, a scavenger of most ROS [23,44,45] (but readily oxidized by $^1O_2$ [25]), exhibited the same inhibitory effect as t-BuOH (Figure 3), further supporting the dominant role of •OH radicals in the PI/H_2O_2 process, at least under acidic conditions. These observations strongly align with results reported for batch operations, as discussed earlier. Kim et al. [17] identified several oxidation intermediates commonly formed during •OH-induced BA oxidation, including dihydroxybenzoic acid, trihydroxybenzoic acid, and hydroxybenzoquinone, providing strong evidence that •OH is the predominant oxidant in the process. Further supporting the hydroxylation capability of •OH, coumarin—used as an indicator of •OH formation—was converted into 7-hydroxycoumarin upon exposure to the PI/H_2O_2 mixture [17]. Additionally, EPR spectral analysis using DMPO and TEMP as spin traps for •OH and $^1O_2$, respectively, indicated that PI reduction by H_2O_2 at pH < 5 predominantly favored the formation of •OH over $^1O_2$ [17].

3.4. Dyes Type Impact

Conversion results from runs conducted at pH 5, with a dye–PI stream flow rate of 565 µL/s (25 µM dyes, 1 mM PI) and varying H_2O_2 flow rates from 40 to 120 µL/s, for different dyes [Basic Blue 41 (BB41), Reactive Green 19 (RG19), Rhodamine B (RhB), Direct Red 81 (DR81), Safranin O (SO), and Basic Fuchsin (BF)] of different classes (see Table 2), are depicted in Figure 5. The observed effectiveness of the PI/H_2O_2 process extends beyond Basic Yellow 28 (BY28) to a wide range of dyes, demonstrating its broad applicability. As shown in Figure 5, all tested dyes exhibited significant degradation, with conversion exceeding 60% (and might achieving 95%) at the highest H_2O_2 flow rate (120 µL/s). However, differences in dye structure influenced their conversion efficiency. Mono-azo dyes, including BY28 and BB41, showed the highest reactivity, with conversion increasing from 43.9% and 45.2% (40 µL/s) to 91.3% and 96.8% (120 µL/s), respectively. Di-azo dyes, such as DR81 and RG19, also exhibited strong degradation, though slightly lower than mono-azo dyes. RG19 showed a notable increase in conversion from 45.4% to 82.1% with increasing H_2O_2 dosage, while DR81 exhibited slightly lower conversion values under similar conditions. The presence of two azo bonds may contribute to a relatively more complex degradation pathway, requiring a higher oxidative demand. Meanwhile, triarylmethane (Basic Fuchsin) and xanthene (Rhodamine B) dyes followed a different trend. Rhodamine B displayed improved degradation with increasing H_2O_2, reaching 73.3% at 120 µL/s, while Basic Fuchsin exhibited conversion around 60%, indicating moderate susceptibility to the process. These dyes, with more complex conjugated structures, may undergo alternative degradation pathways that influence their removal rates.

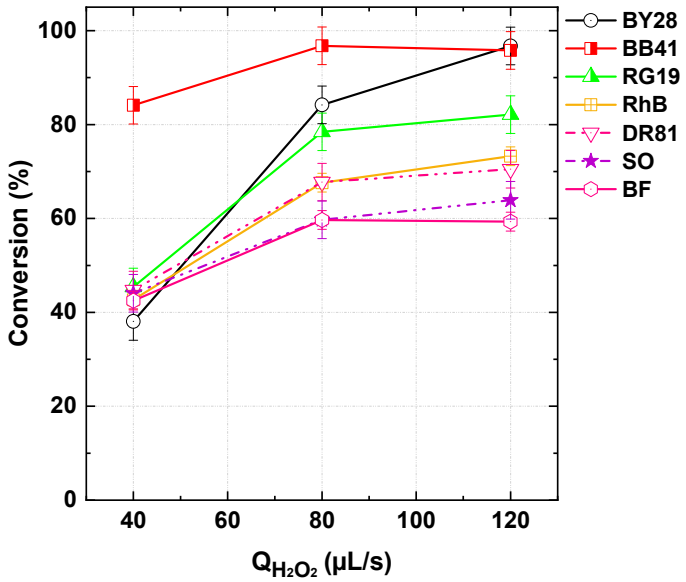


Figure 5. Dyes conversion with the PI/H_2O_2 system in the flowing microreactor as a function of H_2O_2 flow rate at pH 5 of the inlet solution streams (Q_{feed} = 565 µL/s with $C_{dye,in}$ = 25 µM and $[PI]_{in}$ = 1 mM, Reactor length L = 2 m). BY28: Basic Yellow 28. BB41: Basic Blue 41. RG19: Reactive Green 19. RhB: Rhodamine B. DR81: Direct Red 81. SO: Safranin O. BF: Basic Fuchsin.

Among the tested dyes, Safranin O (SO), a phenazine-based dye, demonstrated the lowest degradation efficiency, with conversion increasing from 44.1% (40 µL/s) to 63.9% (120 µL/s). The relatively lower efficiency may be attributed to its stable aromatic structure, which is less susceptible to oxidative attack. Despite these variations, the results confirm the effectiveness of the PI/H_2O_2 process across diverse dye categories, achieving significant removal efficiencies for all tested dyes. The influence of dye structure on process performance highlights the need for further mechanistic analysis to optimize treatment conditions

for different dye types. However, it should be mentioned that the observed differences may also be linked to the dyes' purity, as many of them are sourced from industrial production, where additives and impurities could influence their reactivity and degradation behavior. Understanding the impact of such factors is crucial for accurately assessing the efficiency of the PI/H_2O_2 process in real-world applications.

3.5. Inlet PI and Dye Concentrations/Flow Rates Impact

Figure 6 illustrates the effect of varying inlet PI concentrations (0.5–2 mM) on dye conversion in the flowing microreactor, maintaining a fixed dye flow rate of 565 μL/s and H_2O_2 flow rates of 40, 80, and 120 μL/s. As seen, higher dye conversion was consistently associated with increased PI concentrations. Increasing the inlet PI concentration implies a higher PI flow rate, thereby elevating its concentration in the reaction mixture. This, in turn, leads to a greater generation of reactive radicals through the chain reaction between PI and H_2O_2 (Table 1), enhancing the dye degradation rate. According to Figure 6, complete (100%) dye conversion was achieved with 2 mM PI at just 80 μL/s of H_2O_2. In contrast, at 120 μL/s of H_2O_2, conversion efficiencies of only 91% and 77.8% were recorded for 1 mM and 0.5 mM PI, respectively. A similar trend has been reported in batch reaction systems [17,18,23] while an optimal PI concentration (5 mM) was observed for some cases [23]. The retrieved optimum was attributed to radical quenching caused by excess PI, as described in Reaction (16) of Table 1. However, in our flowing system, an optimum scenario was not observed, likely due to the lower PI concentrations employed in the inlet dye stream (1 mM).

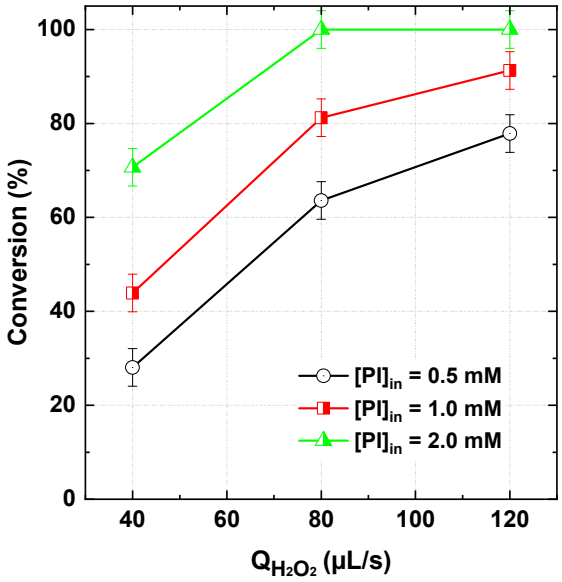


Figure 6. BY28 conversion with the PI/H_2O_2 system in the flowing microreactor as a function of H_2O_2 flow rate at three initial PI inlet concentrations (Q_{dye} = 565 μL/s with $C_{dye,in}$ = 25 μM and $[PI]_{in}$ = 0.5–2 mM, pH_{in} 5, reactor length L = 2 m).

According to Figure 7, a higher conversion rate was associated with lowering initial dye concentration from 50 to 25 μM in the inlet stream. This effect was more pronounced at higher H_2O_2 flow rates (120 μL/s), where 91% of the dye was degraded at 25 μM compared to only 62.6% at 50 μM under the same operating conditions. This trend is expected, as increasing dye concentration can intensify competition between dye molecules and degradation intermediates/by-products—formed in greater quantities at higher dye concentrations—for ROS. This competition limits the direct attack of ROS on dye molecules, thereby reducing the overall process efficiency. A similar behavior has been reported in batch-mode systems [23]. However, an unexpected effect was observed at very low

dye concentrations (12.5 μM), where the conversion rate was lower than that obtained at 25 μM (Figure 7). This trend, which was consistent across all tested H_2O_2 flow rates, can be attributed to the dominance of radical–radical quenching (Equation (6), Table 1) over the reaction between ROS and dye molecules. At low dye concentrations and high ROS availability, the probability of ROS interacting with dye molecules decreases, favoring radical–radical recombination or even radical quenching by the initial oxidants (PI or H_2O_2), as described in reactions (10) and (16) of Table 1.

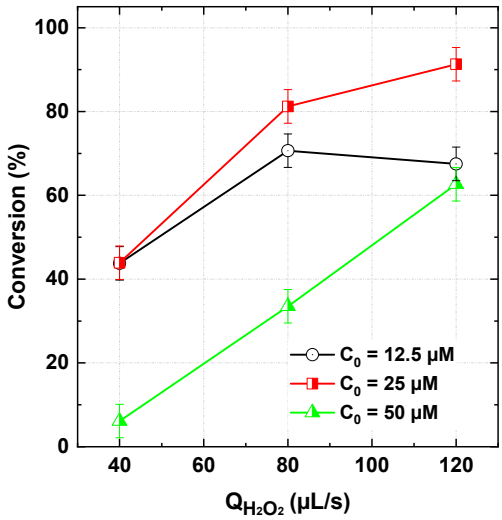


Figure 7. BY28 conversion with the PI/H_2O_2 system in the flowing microreactor as a function of H_2O_2 flow rate at three initial dye concentrations (Q_{dye} = 565 μL/s with $C_{dye,in}$ = 12.5–50 μM and $[PI]_{in}$ = 1 mM, pH_{in} 5, reactor length L = 2 m).

In a subsequent series of runs, the inlet dye–PI flow rate was varied between 278 and 1100 μL/s while maintaining fixed inlet concentrations of PI (1 mM) and dye (25 μM). The results depicted in Figure 8 demonstrated a gradual increase in dye conversion with decreasing dye–PI flow rate. In this operating mode, both dye and PI molar flux were proportionally increased. Except for the case of 278 μL/s at 120 μL/s H_2O_2, the observed trend was consistent: conversion decreased with increasing dye–PI flow rate. This behavior can be attributed to the previously discussed competition mechanism, where degradation intermediates and by-products compete with dye molecules for reactive oxygen species (ROS), thereby limiting the direct oxidation of the dye. In addition, the increase in flow rate reduces the residence time of the reaction mixture, consequently limiting the reaction period available for further degradation, which can negatively impact overall conversion efficiency. However, the lower conversion observed at 278 μL/s (120 μL/s H_2O_2) compared to 565 μL/s (Figure 8) can be explained by the radical–radical quenching mechanism discussed previously for the unexpected impact of the lower initial dye concentration (12.5 μM). In this case, radical–radical interactions effectively compete with radical-dye reactions, leading to enhanced quenching and a significant reduction in radical availability for dye degradation.

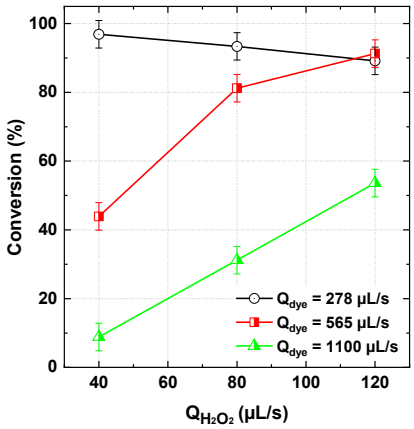


Figure 8. BY28 conversion with the PI/H_2O_2 system in the flowing microreactor as a function of H_2O_2 and dye–PI inlet flow rate (Q_{dye} = 278–1100 µL/s with $C_{dye,in}$ = 25 µM and $[PI]_{in}$ = 1 mM, pH_{in} 5, reactor length L = 2 m).

3.6. Heating Impact

The impact of solution heating on the performance of the flowing reaction system was assessed by controlling the bath temperature, in which the tubular microreactor was submerged, at 25, 35, 45, and 55 °C (Figure 9) under the conditions specified in the figure caption. As observed, increasing the temperature led to a decline in dye conversion, with the reduction becoming more pronounced at higher H_2O_2 flow rates. A similar temperature-dependent trend was reported by Chadi et al. [23] for the degradation of toluidine blue in batch-mode operation. Given the thermal stability of periodate [6], the observed negative effect of elevated temperatures is attributed to the thermodynamic instability of hydrogen peroxide. H_2O_2 undergoes self-decomposition into water and oxygen, as described by Equation (22). An increase of 10 °C is reported to accelerate the decomposition rate of H_2O_2 by a factor of approximately 2.30 [46], which significantly diminishes the availability of oxidants essential for dye degradation. Therefore, operating the flowing microreactor system at lower temperatures is recommended to achieve optimal performance, as it minimizes the thermal decomposition of H_2O_2 and preserves its oxidative capacity.

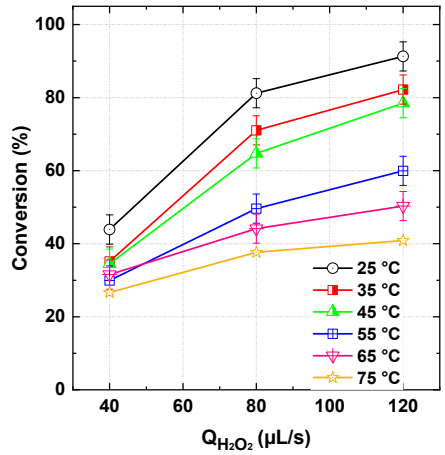


Figure 9. BY28 conversion with the PI/H_2O_2 system in the flowing microreactor as a function of H_2O_2 and bath temperature (Q_{dye} = 278–1100 µL/s with $C_{dye,in}$ = 25 µM and $[PI]_{in}$ = 1 mM, reactor length L = 2 m).

3.7. Reactor Length Impact

The influence of reactor length (2 m vs. 6 m) on dye conversion in the flowing microreactor was assessed under different scenarios: (i) varying the dye–periodate stream

flow rate at a fixed H_2O_2 flow rate (Figure 10a), and (ii) varying the H_2O_2 flow rate at a fixed dye flow rate (Figure 10b). Further operational details are provided in the caption of Figure 10. Across all tested conditions, no significant difference in conversion was observed between the 2 m and 6 m reactor lengths, despite their different residence times—estimated at 3.95 s and 11.84 s, respectively—based on a total flow rate of 398 µL/s (278 µL/s dye + 120 µL/s H_2O_2) and a tubular geometry of 1 mm internal diameter. When increasing the dye flow rate from 278 to 565 and 1100 µL/s while maintaining the H_2O_2 flow rate at 120 µL/s, the residence time decreased to 2.92 s and 1.29 s, respectively. Despite this, the dye conversion remained largely unaffected, which suggests that the reaction kinetics of the PI/H_2O_2 system are extremely rapid. This is consistent with the findings of Chadi et al. [23], who reported nearly instantaneous decolorization of toluidine blue upon periodate activation. Hence, extending the reactor length or residence time offers limited benefit in such fast-reacting systems, as the key reactions are completed within a very short timescale.

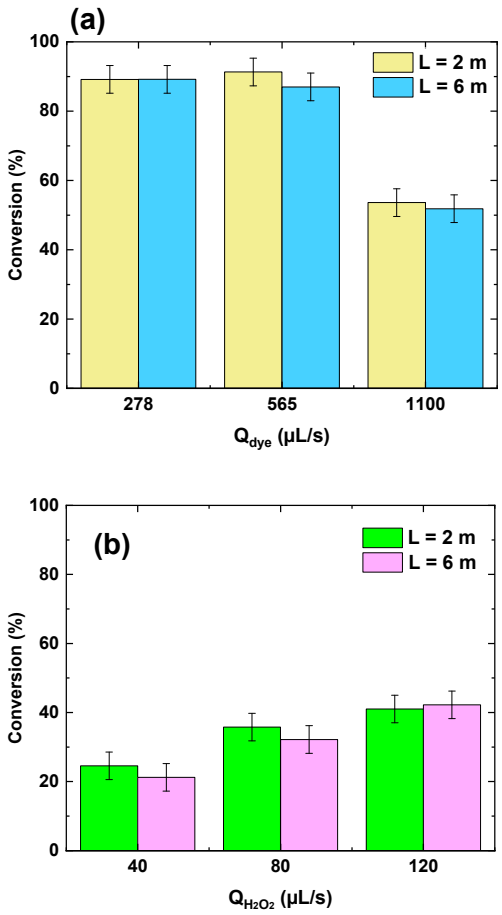


Figure 10. Reactor length (L) effect on BY28 conversion with the PI/H_2O_2 system in the flowing microreactor as a function of H_2O_2 and dye flow rates. (**a**) Q_{H2O2} = 120 µL/s with $[H_2O_2]_0$ = 50 mM, $[PI]_{in}$ = 1 mM, pH 5, (**b**) Q_{dye} = 278 µL/s, $[PI]_0$ = 0.5 mM, $[H_2O_2]_0$ = 10 mM, pH 5. $C_{dye,in}$ = 25 µM and T_{bath} = 25 °C for all runs.

3.8. TOC Reduction in the PI/H_2O_2 System

To comprehensively evaluate the performance of the PI/H_2O_2 system, the study extended beyond dye degradation to assess mineralization efficiency under different operating conditions. Total organic carbon (TOC) reduction was analyzed by varying the dye–PI flow rate (278 and 656 µL/s), the PI dosage (1 and 2 mM), and the H_2O_2 flow rate (0–120 µL/s). The results, summarized in Figure 11, demonstrate the system's potential for

achieving complete mineralization under certain conditions, particularly when the oxidant dosage is appropriately adjusted.

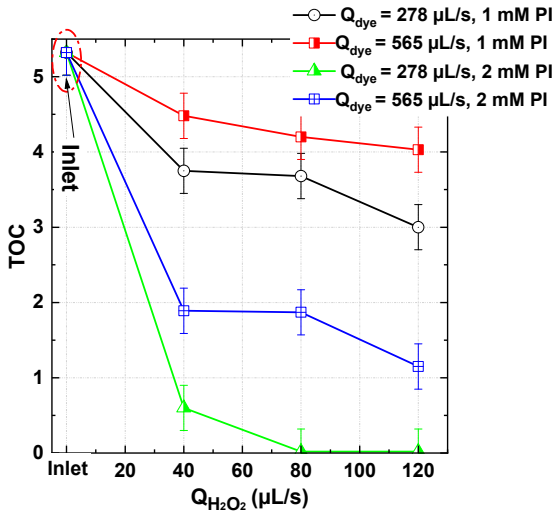


Figure 11. TOC conversion with the PI/H_2O_2 system in the flowing microreactor as a function of H_2O_2 and dye (BY28) flow rates for two PI inlet concentration (1 and 2 mM) and $[H_2O_2]_0$ = 50 mM, pH inlet 5 and bath temperature of 25 °C (Reactor length L = 2 m).

For the case of 1 mM PI/50 mM H_2O_2, TOC reduction followed a moderate trend. At a lower dye–PI flow rate (278 µL/s), TOC values declined from 5.32 mg/L to 3.0 mg/L as H_2O_2 dosage increased to 120 µL/s. However, at a higher dye–PI flow rate (656 µL/s), the final TOC remained at 4.0 mg/L, indicating reduced mineralization efficiency. This suggests that an increased organic load introduces competition between dye molecules and intermediate degradation by-products for ROS, thereby limiting complete oxidation. However, a significant improvement was observed when the PI dosage was increased to 2 mM. Under these conditions, near-total mineralization was achieved at Q_{dye} = 278 µL/s, with TOC dropping from 5.32 mg/L to only 0.02 mg/L at $H_2O_2 \geq 80$ µL/s. At the higher dye–PI flow rate (656 µL/s), TOC reduction was still notable, reaching 1.1 mg/L at the highest oxidant dosage. These results confirm that periodate activation plays a crucial role in enhancing hydroxyl radical generation, leading to improved oxidation and mineralization efficiency. However, at higher organic loads, complete mineralization remains challenging.

Overall, the PI/H_2O_2 process exhibits high mineralization efficiency, particularly under controlled pollutant loads and optimized oxidant dosing. The best performance was achieved at Q_{dye} = 278 µL/s, PI = 2 mM, and $H_2O_2 \geq 80$ µL/s, where nearly complete TOC removal was recorded. These findings highlight the strong potential of the flowing microprocess for wastewater treatment applications, effectively breaking down organic contaminants into CO_2 and H_2O, making it a promising approach for environmental remediation.

3.9. Salts Impact

The influence of various mineral salts, namely NaCl, Na_2SO_4, $NaNO_3$, and $NaHCO_3$ on the conversion of the dye BY28 in the dye–PI stream was investigated across a range of H_2O_2 flow rates (40–120 µL/s). The experiments were primarily conducted at an inlet pH of 5, except for $NaHCO_3$, where additional tests were performed at pH 7 to ensure the presence of HCO_3^- ions in solution. The results are presented in Figure 12.

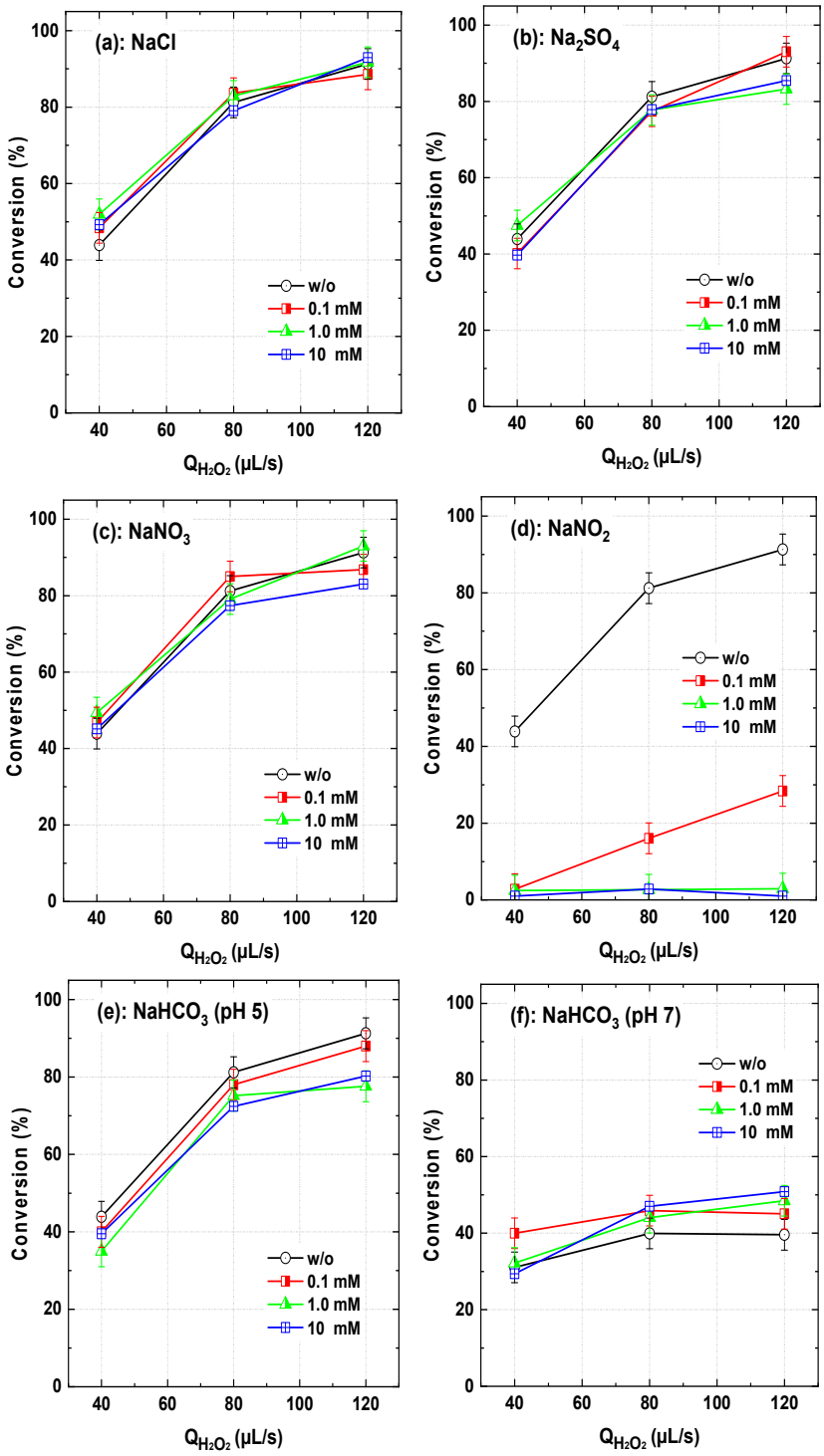


Figure 12. BY28 conversion with the PI/H_2O_2 system in the flowing microreactor as a function of H_2O_2 in the presence of different salts in the dye inlet stream (Q_{dye} = 565 μL/s with $C_{dye,in}$ = 25 μM, $[PI]_{in}$ = 1 mM, and $[Salts]_{in}$ = 0.1–10 mM, pH 5 (except for the (**f**) case where pH is 7), reactor length L = 2 m).

Across the tested range of salts and H_2O_2 flow rates, chloride, nitrate, and sulfate exhibited no significant impact on dye conversion. This partially aligns with their behavior in batch-mode experiments. In fact, Chadi et al. [23] reported a 15–20% reduction in the degradation of Toluidine Blue in the presence of 10 mM NaCl, Na_2SO_4, and $NaNO_3$, with more pronounced effects at 50 mM. Sulfate is generally considered inert in most •OH-based AOPs [10,41,47,48]. Although Cl^- and NO_3^- are known to react with •OH, forming less

reactive radicals such as $Cl^{\bullet}$, $Cl_2^{\bullet-}$, and $NO_3^{\bullet}$ (Reactions (27)–(30)), their effect in the continuous-flow system remained marginal. This could be attributed to the lower reactivity of chlorine radicals toward Basic Yellow 10 compared to Toluidine Blue.

$$Cl^- + {}^{\bullet}OH \rightarrow ClOH^{\bullet-} \qquad k_{27} = 4.3 \times 10^9\ M^{-1}s^{-1} \tag{27}$$

$$ClOH^{\bullet-} \rightarrow Cl^{\bullet} + OH^- \qquad k_{28} = 2.1 \times 10^{10}\ M^{-1}s^{-1} \tag{28}$$

$$Cl^{\bullet} + Cl^- \rightleftharpoons Cl_2^{\bullet-} \qquad k_{29} = (5.6\text{–}12) \times 10^9\ M^{-1}s^{-1},\ k_{-29} = (6\text{–}11) \times 10^4\ M^{-1}s^{-1} \tag{29}$$

$$NO_3^- + {}^{\bullet}OH \rightarrow NO_3^{\bullet} + OH^- \tag{30}$$

In contrast, nitrite (NO_2^-) significantly inhibited dye conversion, as shown in Figure 12c. Even at concentrations as low as 1 mM, nitrite completely quenched the reaction. This is attributed to its higher reactivity toward $^{\bullet}OH$ (Equation (31)) compared to nitrate. Similar effects have been reported in Fe(II)/chlorine, Fe(III)/chlorine, and UV/chlorine systems, where $^{\bullet}OH$ and reactive chlorine species play a crucial role in the degradation process [42,48,49].

$$NO_2^- + {}^{\bullet}OH \rightarrow OH^- + NO_2^{\bullet} \quad k_{31} = 1 \times 10^{10}\ M^{-1}s^{-1} \tag{31}$$

The impact of bicarbonate (HCO_3^-) was particularly notable. At pH 5, bicarbonate had a marginal to slight inhibitory effect, reducing dye conversion by up to 12% at 10 mM (Figure 12e). However, at pH 7, an enhancement of 10–12% was observed. This behavior is linked to bicarbonate chemistry and its pH-dependent speciation. Bicarbonate reacts with $^{\bullet}OH$ to produce carbonate radicals ($CO_3^{\bullet-}$, Equation (32)), which, although more selective than hydroxyl radicals, remain reactive toward organic dyes (E^0 = 1.78 V vs. 2.8 V for $^{\bullet}OH$), particularly under neutral to slightly alkaline conditions [41]:

$$HCO_3^- + {}^{\bullet}OH \rightarrow CO_3^{\bullet-} + H_2O \qquad k_{32} = 8.5 \times 10^6\ M^{-1}s^{-1} \tag{32}$$

Several studies have highlighted carbonate radical-induced enhancement in $^{\bullet}OH$-based AOPs. Merouani et al. [41] demonstrated that bicarbonate significantly accelerated the sonochemical degradation of Rhodamine B at pH 8.4. Similar findings were reported by Pétrier et al. for Bisphenol A and pharmaceutical pollutants [47,50,51]. he self-recombination of $CO_3^{\bullet-}$ (Equation (33)) is 275 times slower than that of $^{\bullet}OH$, resulting in a longer lifetime for $CO_3^{\bullet-}$ and greater interaction with the dye molecules [41,47]. Consequently, low concentrations of HCO_3^- can enhance degradation, whereas higher concentrations may inhibit oxidation efficiency in H_2O_2/IO_4^--AOP.

$$CO_3^{\bullet-} + CO_3^{\bullet-} \rightarrow CO_2 + CO_4^{2-} \quad k_{33} = 1.5 \times 10^7\ M^{-1}\ s^{-1} \tag{33}$$

At pH 5, the impact of bicarbonate can be attributed to its speciation equilibrium. Given the pK_a values of carbonic acid (6.35 and 10.33), bicarbonate predominates in the pH range 6–10, while CO_2 (carbonic acid) dominates at pH < 6. At pH 5, most carbonate species exist as dissolved CO_2, which does not generate $CO_3^{\bullet-}$, explaining the minor inhibition observed. In contrast, at pH 7, HCO_3^- is the dominant species, leading to enhanced degradation efficiency through the generation of $CO_3^{\bullet-}$ radicals.

3.10. Organic Matters Impact

Surfactants are commonly used as additives in dyeing processes and are frequently released into wastewater along with dye residues, with reported levels ranging from a few micrograms to several milligrams per liter [52–54], depending on the processing steps,

types of dyes and auxiliaries used, and the treatment practices implemented. Similarly, sucrose and glucose are prevalent organic compounds in municipal wastewater effluents. Given their widespread presence, the impact of selected surfactants—Triton X-100, sodium dodecyl sulfate (SDS), Tween 20, and Tween 80—along with sucrose and glucose on the performance of the flowing H_2O_2/IO_4^- process for TBY28 degradation was investigated. The effects of sucrose and glucose (0.1–10 mM) and surfactants (100 µM) on dye oxidation were evaluated at pH 5 in the continuous-flow system, with results presented in Figure 13a and 13b, respectively, across varying H_2O_2 flow rates.

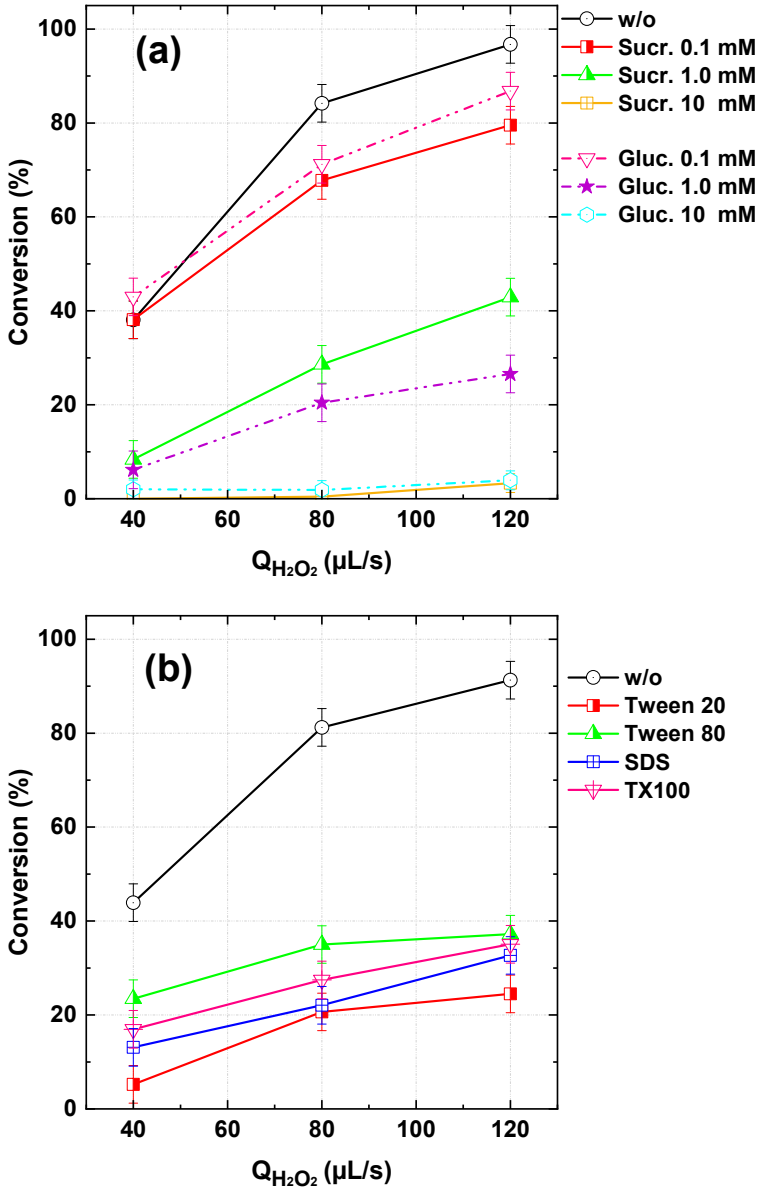


Figure 13. BY28 conversion with the PI/H_2O_2 system in the flowing microreactor as a function of H_2O_2 flow rate in the presence of different organic matters in the dye inlet stream. (**a**) Sucrose and glucose and (**b**) surfactants (Q_{dye} = 565 µL/s with $C_{dye,in}$ = 25 µM, $[PI]_{in}$ = 1 mM, and $[OM]_{in}$ = 0.1–10 for sucrose and glucose and 100 µm for surfactants, pH_{in} 5, Reactor length L = 2 m). OM: organic matter (sucrose, glucose, surfactants).

All tested surfactants exhibited a quenching effect on the dye degradation process (Figure 13b). Among them, Tween 20 demonstrated the least inhibitory impact, followed by Triton X-100, SDS, and finally Tween 80, which showed the highest suppression of dye conversion. Similarly, glucose and sucrose significantly reduced the treatment efficiency

of BY28 (Figure 13a), with their inhibitory effects becoming particularly pronounced at higher concentrations (10 mM), where nearly complete suppression of dye degradation (~100%) was observed. These inhibitory effects can be attributed to the high reactivity of surfactants, sucrose, and glucose toward •OH, the primary reactive species in the system. For instance, the reported second-order rate constants for the reactions of •OH with Triton X-100, glucose, and sucrose are (8.8–9.6) $\times$ 10^9 $M^{-1}s^{-1}$, 1.5 $\times$ 10^9 $M^{-1}s^{-1}$, and 3.2 $\times$ 10^9 $M^{-1}s^{-1}$, respectively [40]. Consequently, the presence of these organic compounds leads to significant competition for •OH, thereby inhibiting BY28 degradation (Figure 13). Similar findings were reported by Chadi et al. [23] for the removal of Toluidine Blue in batch reaction systems.

3.11. Water Quality Impact

Water quality plays a critical role in determining the efficiency of AOPs. To evaluate this effect, different real water matrices—including seawater, tap water, river water, and secondary effluents from a municipal wastewater treatment plant (SEWWTP)—were used as solvents for dissolving BY28 and conducting reference experiments in the continuous-flow PI/H_2O_2 microreactor system. The results, presented in Figure 14, revealed the following inhibition trend: tap water < seawater < SEWWTP < river water. The stronger inhibitory effects observed with SEWWTP and river water were attributed to their high content of organic matter, which competes with the dye for ROS, thereby reducing oxidation efficiency. Conversely, tap water exhibited the least inhibition due to its lower salt content and the absence of significant organic matter (Table 3), thereby minimizing competition for ROS scavenging.

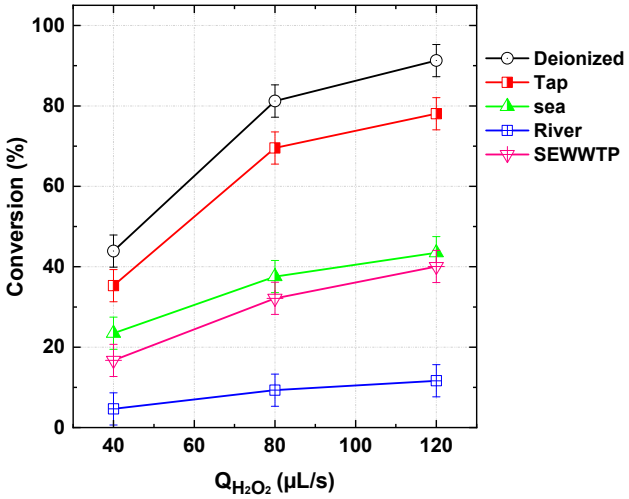


Figure 14. Impact of different water matrices on BY28 conversion by PI/H_2O_2 system in the flowing microreactor as a function of H_2O_2 flow rate (Q_{dye} = 565 µL/s with $C_{dye,in}$ = 25 µM, $[PI]_{in}$ = 1 mM, pH 5, reactor length L = 2 m).

Although seawater contains a high concentration of salts, particularly chloride (20 g/L), it remained viable for BY28 degradation. The process performance in seawater could be further optimized by adjusting operational parameters, such as reactant dosages, to mitigate potential scavenging effects. These findings highlight the importance of water matrix composition in AOP efficiency, particularly the presence of organic and inorganic constituents that can influence ROS availability. Future optimization strategies should focus on tailoring operational conditions to specific water types, ensuring the robustness of the process for real wastewater treatment applications.

4. Conclusions

This study evaluated the effectiveness of the H_2O_2/IO_4^- process for degrading textile dyes under continuous-flow conditions. The results demonstrated that the process is highly efficient, with hydroxyl radicals playing a dominant role in dye oxidation. The influence of various organic and inorganic constituents, including surfactants, carbohydrates, and different water matrices, was systematically examined to assess their impact on treatment performance.

The findings revealed that the efficiency of dye degradation and mineralization strongly depends on flow conditions and reactant concentrations. Higher conversion yields were achieved at increased H_2O_2 flow rates, higher periodate (PI) dosages, and lower initial dye concentrations. Complete mineralization was attainable with 2 mM PI at H_2O_2 flow rates of 80 and 120 µL/s. Reactor length had no significant impact on process performance, while temperature increases led to a decline in treatment efficiency. Surfactants and organic compounds such as sucrose and glucose exhibited strong inhibitory effects on BY28 degradation due to their high reactivity with $^{\bullet}OH$. At elevated concentrations (10 mM), sucrose and glucose nearly suppressed the oxidation process, highlighting the importance of accounting for organic loads in real wastewater applications. Water quality analysis further emphasized the variability in process efficiency across different real matrices. While tap water exhibited minimal inhibition, SEWWTP and river water significantly reduced degradation efficiency due to their high organic matter content, which competes with ROS. Notably, despite its high salt content, seawater remained a viable medium for dye degradation, suggesting that process performance in saline environments could be further optimized by adjusting operational parameters.

Although microreactors are not designed for large-scale wastewater treatment due to throughput limitations, their use in this study provided a highly controlled and reproducible environment for investigating the rapid kinetics and mechanistic behavior of the PI/H_2O_2 system. This approach enabled precise tuning of residence time, flow regime, and reagent distribution—critical aspects for elucidating fundamental reaction pathways in advanced oxidation processes. The insights gained here lay the groundwork for future translation into scalable reactor architectures such as meso- or millifluidic systems with improved energy and process efficiency.

Overall, these results underscore the critical role of both organic and inorganic constituents in determining the efficiency of AOPs for dye removal. Future research should focus on refining process conditions to mitigate the inhibitory effects of competing organic and inorganic species, while also exploring scalable reactor designs to support industrial and municipal applications of the H_2O_2/IO_4^- system.

Author Contributions: Conceptualization, S.M.; validation, S.M.; formal analysis, S.M.; investigation, A.T.; resources, A.T.; writing—original draft, S.M.; writing—review and editing, A.D.; visualization, S.M. and A.D.; supervision, S.M.; project administration, S.M. All authors have read and agreed to the published version of the manuscript.

Funding: This research received no external funding.

Data Availability Statement: The original contributions presented in this study are included in the article. Further inquiries can be directed to the corresponding author.

Conflicts of Interest: The authors declare no conflict of interest.

References

1. Price, C.; Kroll, H. The Kinetics of the Periodate Oxidation of 1,2-Glycols. *J. Am. Chem. Soc.* **1938**, *60*, 2726–2729. [CrossRef]
2. Galletti, P.; Martelli, G.; Prandini, G.; Colucci, C.; Giacomini, D. Sodium periodate/TEMPO as a selective and efficient system for amine oxidation. *RSC Adv.* **2018**, *8*, 9723–9730. [CrossRef]

3. Sudalai, A.; Khenkin, A.; Neumann, R. Sodium periodate mediated oxidative transformations in organic synthesis. *Org. Biomol. Chem.* **2015**, *13*, 4374–4394. [CrossRef]
4. Yang, T.; Zeng, G.; Jiang, M.; Su, P.; Liu, C.; Lv, Q.; Li, W.; Hou, X.; Li, J. Matching periodate peak absorbance by far UVC at 222 nm promotes the degradation of micropollutants and energy efficiency. *J. Hazard. Mater.* **2024**, *476*, 134978. [CrossRef] [PubMed]
5. Pennington, D.; Ritter, D. Periodate oxidation of phenols. *J. Am. Chem. Soc.* **1947**, *69*, 187. [CrossRef]
6. Bendjama, H.; Merouani, S.; Hamdaoui, O.; Bouhelassa, M. Efficient degradation method of emerging organic pollutants in marine environment using UV/periodate process: Case of chlorazol black. *Mar. Pollut. Bull.* **2018**, *126*, 557–564. [CrossRef] [PubMed]
7. Chia, L.-H.H.; Tang, X.; Weavers, L.K. Kinetics and mechanism of photoactivated periodate reaction with 4-chlorophenol in acidic solution. *Environ. Sci. Technol.* **2004**, *38*, 6875–6880. [CrossRef]
8. Yun, E.T.; Yoo, H.Y.; Kim, W.; Kim, H.E.; Kang, G.; Lee, H.; Lee, S.; Park, T.; Lee, C.; Kim, J.H.; et al. Visible-light-induced activation of periodate that mimics dye-sensitization of TiO_2: Simultaneous decolorization of dyes and production of oxidizing radicals. *Appl. Catal. B Environ.* **2017**, *203*, 475–484. [CrossRef]
9. Li, X.; Liu, X.; Lin, C.; Qi, C.; Zhang, H.; Ma, J. Enhanced activation of periodate by iodine-doped granular activated carbon for organic contaminant degradation. *Chemosphere* **2017**, *181*, 609–618. [CrossRef]
10. Belghit, A.; Merouani, S.; Dehane, A. Exploring the intensifying effect of periodate/hydroxylamine oxidation process for the effective mineralization of textile dyes effluents with consideration of environmental matrices. *Asia-Pac. J. Chem. Eng.* **2024**, *19*, e2981. [CrossRef]
11. Tang, X.; Weavers, L.K. Using photoactivated periodate to decompose TOC from hydrolysates of chemical warfare agents. *J. Photochem. Photobiol. A Chem.* **2008**, *194*, 212–219. [CrossRef]
12. Niu, L.; Zhang, K.; Jiang, L.; Zhang, M.; Feng, M. Emerging periodate-based oxidation technologies for water decontamination: A state-of-the-art mechanistic review and future perspectives. *J. Environ. Manag.* **2022**, *323*, 116241. [CrossRef]
13. Sukhatskiy, Y.; Shepida, M.; Sozanskyi, M.; Znak, Z.; Gogate, P.R. Periodate-based advanced oxidation processes for wastewater treatment: A review. *Sep. Purif. Technol.* **2023**, *304*, 122305. [CrossRef]
14. Yang, B.; Ma, Q.; Hao, J.; Huang, J.; Wang, Q.; Wang, D.; Zhang, J. Periodate-based advanced oxidation processes: A review focusing on the overlooked role of high-valent iron and manganese species. *Chemosphere* **2023**, *337*, 139442. [CrossRef]
15. Sun, H.; He, F.; Choi, W. Production of Reactive Oxygen Species by the Reaction of Periodate and Hydroxylamine for Rapid Removal of Organic Pollutants and Waterborne Bacteria. *Environ. Sci. Technol.* **2020**, *54*, 6427–6437. [CrossRef] [PubMed]
16. Du, J.; Xiao, G.; Xi, Y.; Zhu, X.; Su, F.; Kim, S.H. Periodate activation with manganese oxides for sulfanilamide degradation. *Water Res.* **2020**, *169*, 115278. [CrossRef]
17. Kim, Y.; Lee, H.; Oh, H.; Haider, Z.; Choi, J.; Shin, Y.U.; Kim, H.; Lee, J. Revisiting the Oxidizing Capacity of the Periodate-H_2O_2 Mixture: Identification of the Primary Oxidants and Their Formation Mechanisms. *Environ. Sci. Technol.* **2022**, *56*, 5763–5774. [CrossRef]
18. Chen, T.; Sun, Y.; Dong, H.; Chen, J.; Yu, Y.; Ao, Z.; Guan, X. Understanding the Importance of Periodate Species in the pH-Dependent Degradation of Organic Contaminants in the H_2O_2/Periodate Process. *Environ. Sci. Technol.* **2022**, *56*, 10372–10380. [CrossRef]
19. Lee, Y.C.; Chen, M.J.; Huang, C.P.; Kuo, J.; Lo, S.L. Efficient sonochemical degradation of perfluorooctanoic acid using periodate. *Ultrason. Sonochem.* **2016**, *31*, 499–505. [CrossRef]
20. Du, J.; Tang, S.; Faheem; Ling, H.; Zheng, H.; Xiao, G.; Luo, L.; Bao, J. Insights into periodate oxidation of bisphenol A mediated by manganese. *Chem. Eng. J.* **2019**, *369*, 1034–1039. [CrossRef]
21. Zong, Y.; Shao, Y.; Zeng, Y.; Shao, B.; Xu, L.; Zhao, Z.; Liu, W.; Wu, D. Enhanced Oxidation of Organic Contaminants by Iron(II)-Activated Periodate: The Significance of High-Valent Iron-Oxo Species. *Environ. Sci. Technol.* **2021**, *55*, 7634–7642. [CrossRef]
22. Lee, H.; Yoo, H.Y.; Choi, J.; Nam, I.H.; Lee, S.; Lee, S.; Kim, J.H.; Lee, C.; Lee, J. Oxidizing capacity of periodate activated with iron-based bimetallic nanoparticles. *Environ. Sci. Technol.* **2014**, *48*, 8086–8093. [CrossRef]
23. Chadi, N.E.; Merouani, S.; Hamdaoui, O.; Bouhelassa, M.; Ashokkumar, M. H_2O_2/Periodate (IO_4^-): A novel advanced oxidation technology for the degradation of refractory organic pollutants. *Environ. Sci. Water Res. Technol.* **2019**, *5*, 1113–1123. [CrossRef]
24. Chadi, N.E.; Merouani, S.; Hamdaoui, O.; Bouhelassa, M.; Ashokkumar, M. Influence of mineral water constituents, organic matter and water matrices on the performance of the H_2O_2/IO_4^--advanced oxidation process. *Environ. Sci. Water Res. Technol.* **2019**, *5*, 1985–1992. [CrossRef]
25. Zhou, Y.; Jiang, J.; Gao, Y.; Ma, J.; Pang, S.-Y.; Li, J.; Lu, X.-T.; Yuan, L.-P. Activation of Peroxymonosulfate by Benzoquinone: A Novel Nonradical Oxidation Process. *Environ. Sci. Technol.* **2015**, *49*, 12941–12950. [CrossRef] [PubMed]
26. Bokare, A.D.; Choi, W. Singlet-Oxygen generation in alkaline periodate solution. *Environ. Sci. Technol.* **2015**, *49*, 14392–14400. [CrossRef] [PubMed]

27. Nge, P.N.; Rogers, C.I.; Woolley, A.T. Advances in microfluidic materials, functions, integration, and applications. *Chem. Rev.* **2013**, *113*, 2550–2583. [CrossRef]
28. Dong, G.; Chen, B.; Liu, B.; Hounjet, L.J.; Cao, Y.; Stoyanov, S.R.; Yang, M.; Zhang, B. Advanced oxidation processes in microreactors for water and wastewater treatment: Development, challenges, and opportunities. *Water Res.* **2022**, *211*, 118047. [CrossRef]
29. Cambié, D.; Bottecchia, C.; Straathof, N.J.W.; Hessel, V.; Noël, T. Applications of Continuous-Flow Photochemistry in Organic Synthesis, Material Science, and Water Treatment. *Chem. Rev.* **2016**, *116*, 10276–10341. [CrossRef]
30. Babakir, B.A.M.; Abd Ali, L.I.; Ismail, H.K. Rapid removal of anionic organic dye from contaminated water using a poly(3-aminobenzoic acid/graphene oxide/cobalt ferrite) nanocomposite low-cost adsorbent via adsorption techniques. *Arab. J. Chem.* **2022**, *15*, 104318. [CrossRef]
31. Feng, C.; Ren, P.; Huo, M.; Dai, Z.; Liang, D.; Jin, Y.; Ren, F. Facile synthesis of trimethylammonium grafted cellulose foams with high capacity for selective adsorption of anionic dyes from water. *Carbohydr. Polym.* **2020**, *241*, 116369. [CrossRef] [PubMed]
32. Zhou, Z.; Ye, G.; Zong, Y.; Zhao, Z.; Hou, C.; Chen, Z.; Wu, D. Revisiting the role of H_2O_2 in periodate electro-activation system: The non-dependence in Bisphenol A (BPA) removal. *Sep. Purif. Technol.* **2025**, *352*, 128090. [CrossRef]
33. Guo, X.-H.; Ma, G.-W.; Wang, X.-Y.; Gai, W.-Z.; Deng, Z.-Y. Al-water reaction generates metastable aluminum cluster ions and their use in advanced oxidation processes. *Sep. Purif. Technol.* **2024**, *349*, 127838. [CrossRef]
34. Nidheesh, P.V.; Khatri, J.; Anantha Singh, T.S.; Gandhimathi, R.; Ramesh, S.T. Review of zero-valent aluminium based water and wastewater treatment methods. *Chemosphere* **2018**, *200*, 621–631. [CrossRef] [PubMed]
35. Shah, S.N.A.; Li, H.; Lin, J.M. Enhancement of periodate-hydrogen peroxide chemiluminescence by nitrogen doped carbon dots and its application for the determination of pyrogallol and gallic acid. *Talanta* **2016**, *153*, 23–30. [CrossRef]
36. Weavers, L.K.; Hua, I.; Hoffmann, M.R. Degradation of triethanolamine and chemical oxygen demand reduction in wastewater by photoactivated periodate. *Water Environ. Res.* **1997**, *69*, 1112–1119. [CrossRef]
37. Lee, C.; Yoon, J. Application of photoactivated periodate to the decolorization of reactive dye: Reaction parameters and mechanism. *J. Photochem. Photobiol. A Chem.* **2004**, *165*, 35–41. [CrossRef]
38. Yoon, S.H.; Lee, S.; Kim, T.H.; Lee, M.; Yu, S. Oxidation of methylated arsenic species by UV/$S_2O_8^{2-}$. *Chem. Eng. J.* **2011**, *173*, 290–295. [CrossRef]
39. Merouani, S.; Hamdaoui, O.; Saoudi, F.; Chiha, M. Influence of experimental parameters on sonochemistry dosimetries: KI oxidation, Fricke reaction and H_2O_2 production. *J. Hazard. Mater.* **2010**, *178*, 1007–1014. [CrossRef]
40. Buxton, G.V.; Greenstock, C.L.; Helman, W.P.; Ross, A.B. Critical review of rate constants for reactions of hydrated Electrons, hydrogen atoms and hydroxyl radicals ($^{\bullet}OH/O^{\bullet-}$) in aqueous solution. *J. Phys. Chem. Ref. Data* **1988**, *17*, 515–886. [CrossRef]
41. Merouani, S.; Hamdaoui, O.; Saoudi, F.; Chiha, M.; Pétrier, C. Influence of bicarbonate and carbonate ions on sonochemical degradation of Rhodamine B in aqueous phase. *J. Hazard. Mater.* **2010**, *175*, 593–599. [CrossRef]
42. Belghit, A.A.; Merouani, S.; Hamdaoui, O.; Bouhelassa, M.; Al-Zahrani, S. The multiple role of inorganic and organic additives in the degradation of reactive green 12 by UV/chlorine advanced oxidation process. *Environ. Technol.* **2022**, *43*, 835–847. [CrossRef] [PubMed]
43. Bendjama, H.; Merouani, S.; Hamdaoui, O.; Bouhelassa, M. Using photoactivated acetone for the degradation of Chlorazol Black in aqueous solutions: Impact of mineral and organic additives. *Sci. Total Environ.* **2019**, *653*, 833–838. [CrossRef] [PubMed]
44. Xue, W.; Lin, Z.; Chen, H.; Lu, C.; Lin, J.M. Enhancement of ultraweak chemiluminescence from reaction of hydrogen peroxide and bisulfite by water-soluble carbon nanodots. *J. Phys. Chem. C* **2011**, *115*, 21707–21714. [CrossRef]
45. Chen, H.; Lin, L.; Lin, Z.; Guo, G.; Lin, J.M. Chemiluminescence Arising from the decomposition of peroxymonocarbonate and enhanced by CdTe quantum dots. *J. Phys. Chem. A* **2010**, *114*, 10049–10058. [CrossRef] [PubMed]
46. Wright, W.M. The thermal decomposition of hydrogen peorxyde. *J. Phys. Chem.* **1928**, *31*, 1352–1356.
47. Pétrier, C.; Torres-Palma, R.; Combet, E.; Sarantakos, G.; Baup, S.; Pulgarin, C. Enhanced sonochemical degradation of bisphenol-A by bicarbonate ions. *Ultrason. Sonochem.* **2010**, *17*, 111–115. [CrossRef]
48. Meghlaoui, F.Z.; Merouani, S.; Hamdaoui, O.; Bouhelassa, M.; Ashokkumar, M.; Zohra Meghlaoui, F.; Merouani, S.; Hamdaoui, O.; Bouhelassa, M.; Ashokkumar, M. Rapid catalytic degradation of refractory textile dyes in Fe (II)/chlorine system at near neutral pH: Radical mechanism involving chlorine radical anion ($Cl_2^{\bullet-}$)-mediated transformation pathways and impact of environmental matrices. *Sep. Purif. Technol.* **2019**, *227*, 115685. [CrossRef]
49. Meghlaoui, F.Z.; Merouani, S.; Hamdaoui, O.; Alghyamah, A.; Bouhelassa, M.; Ashokkumar, M. Fe(III)-catalyzed degradation of persistent textile dyes by chlorine at slightly acidic conditions: The crucial role of $Cl_2^{\bullet-}$ radical in the degradation process and impacts of mineral and organic competitors. *Asia-Pacific J. Chem. Eng.* **2020**, *16*, e2553. [CrossRef]
50. Guzman-Duque, F.; Pétrier, C.; Pulgarin, C.; Penuuela, G.; Torres-Palma, R.A. Effects of sonochemical parameters and inorganic ions during the sonochemical degradation of crystal violet in water. *Ultrason. Sonochem.* **2011**, *18*, 440–446. [CrossRef]

51. Villegas-Guzman, P.; Silva-Agredo, J.; Giraldo-Aguirre, A.L.; Florez-Acosta, O.; Petrier, C.; Torres-Palma, R.A.; Florez-Acosta, O.; Petrier, C.; Torres-Palma, R.A.; Flórez-Acosta, O.; et al. Enhancement and inhibition effects of water matrices during the sonochemical degradation of the antibiotic dicloxacillin. *Ultrason. Sonochem.* **2015**, *22*, 211–219. [CrossRef] [PubMed]
52. González, S.; Petrović, M.; Radetic, M.; Jovancic, P.; Ilic, V.; Barceló, D. Characterization and quantitative analysis of surfactants in textile wastewater by liquid chromatography/quadrupole-time-of-flight mass spectrometry. *Rapid Commun. Mass Spectrom.* **2008**, *22*, 1445–1454. [CrossRef] [PubMed]
53. Palmer, M.; Hatley, H. The role of surfactants in wastewater treatment: Impact, removal and future techniques: A critical review. *Water Res.* **2018**, *147*, 60–72. [CrossRef] [PubMed]
54. Araújo, S.; Damianovic, M.; Foresti, E.; Florencio, L.; Kato, M.T.; Gavazza, S. Biological treatment of real textile wastewater containing sulphate, salinity, and surfactant through an anaerobic-aerobic system. *Water Sci. Technol.* **2022**, *85*, 2882–2898. [CrossRef]

Disclaimer/Publisher's Note: The statements, opinions and data contained in all publications are solely those of the individual author(s) and contributor(s) and not of MDPI and/or the editor(s). MDPI and/or the editor(s) disclaim responsibility for any injury to people or property resulting from any ideas, methods, instructions or products referred to in the content.